

Comparison of flux creep and nonlinear $E - j$ approach for analysis of vortex motion in superconductors

D. V. Shantsev^{1,2}, A. V. Bobyl^{1,2}, Y. M. Galperin^{1,2}, and T. H. Johansen^{1,*}

¹*Department of Physics, University of Oslo, P. O. Box 1048 Blindern, 0316 Oslo, Norway*

²*A. F. Ioffe Physico-Technical Institute, Polytekhnicheskaya 26, St.Petersburg 194021, Russia*

Two commonly accepted approaches for simulations of thermally-activated vortex motion in superconductors are compared. These are (i) the so-called flux creep approach based on the expression $E = vB$ relating the electric field E to the velocity v of the thermally-activated flux motion and the local flux density B , and (ii) the approach employing a phenomenological nonlinear current-voltage curve, $E(j)$. Our results show that the two approaches give similar but also distinctly different behaviors for the distributions of current and flux density in both a long slab and thin strip geometry. The differences are most pronounced where the local B is small. Magneto-optical imaging of a $\text{YBa}_2\text{Cu}_3\text{O}_{7-\delta}$ thin film carrying a transport current was performed to compare the simulations with experimental behavior. It is shown that the flux creep approach describes the experiments far better than simulations based on the $E(j)$ approach.

PACS numbers: 74.25.Ha, 74.60.Ge, 74.76.Bz

I. INTRODUCTION

The term *flux creep* is used to describe a thermally-activated motion of flux lines in superconductors. This motion is characterized by a velocity strongly dependent on the local current density. In high-temperature superconductors (HTSCs), the flux creep can be specially pronounced because of small flux pinning energies and high temperatures.^{1,2} An account of the flux creep is therefore crucially important for understanding the time-dependent magnetic behavior of HTSCs. In the literature one finds numerous papers making use of flux creep analysis to describe the evolution of flux and current density distributions, current-voltage curves, magnetization and magnetic susceptibilities for superconductors of various shapes.³⁻⁷

Interestingly, there exist today two commonly accepted approaches for the analysis of thermally-activated flux motion. The first one, the so-called *flux creep* approach, assumes a particular microscopic pinning mechanism, which defines the pinning energy U and its dependence on the local values of current density j and flux density B . The velocity of the thermally-activated flux motion, v , then determines the local electric field according to $E = vB$. The second approach, on the other hand, employs a phenomenological nonlinear current-voltage relation, $E(j)$. For brevity, we will call this the $E - j$ approach.

The present paper is devoted to a detailed comparison of these two approaches. We carry out numerical simulations for the most conventional choice of $E(j)$ and $U(j, B)$ and set focus on the clear differences in the resulting behavior. The numerical findings are then compared to current density distributions measured in YBaCuO films using magneto-optical imaging of flux density profiles. Distinct features in the observed current distributions allow us to conclude which approach gives the more realistic description.

II. THE TWO APPROACHES

To compare the two approaches we consider a one-dimensional flux creep problem where the flux moves along the **x** direction, the magnetic induction **B** is directed along the **z**-axis, while the electric field **E** is parallel to the **y**-axis. The Maxwell equation has then the form

$$\frac{\partial B}{\partial t} = -\frac{\partial E}{\partial x}. \quad (1)$$

In the flux creep approach, since it represents an activation process, the velocity of the vortex motion is given by

$$v = v_c e^{-U(j, B)/kT}, \quad (2)$$

where v_c is the velocity when $U = 0$. In the case that the pinning energy has a logarithmic dependence on the current, $U(j, B) = U_c \ln(j_{cU}/j)$, it follows that the electric field equals

$$E = v_c B (j/j_{cU})^{U_c/kT}. \quad (3)$$

In the $E - j$ approach, the phenomenological $E(j)$ relation is usually chosen in the power law form,

$$E = E_c (j/j_{cE})^n, \quad (4)$$

with $n \gg 1$, and where j_{cE} and E_c are constants with dimension of current density and electric field, respectively.

Comparing Eqs. (4) and (3) one can see that the exponent n in the $E - j$ approach plays the same role as the ratio U_c/kT in the flux creep model. However, even if $n = U_c/kT$, there still remains an important difference. In Eq. (3) one has $E \propto B$, i.e., the electric field induced by the vortex motion is proportional to the number of

moving vortices. In the $E - j$ approach, Eq. (4), this proportionality is absent. As a result, the two approaches become *different* if all parameters, j_{cU} , j_{cE} , and E_c are *independent* of B , which is the conventional assumption.⁸

In the $E - j$ approach at $n \rightarrow \infty$ the electric field tends to zero for $j < j_{cE}$, while it becomes infinitely large for $j > j_{cE}$. This situation is equivalent to the critical-state model characterized by the critical current density j_{cE} . Similarly, for $U_c/kT \rightarrow \infty$ the flux creep approach reproduces the critical-state model with critical current density j_{cU} . Therefore, in the limit $U_c/kT, n \rightarrow \infty$, and $j_{cU} = j_{cE}$ both approaches become equivalent. Accordingly, their difference is expected to grow as n and U_c/kT becomes smaller.

To complete the set of equations one needs also a relation between the flux and current density. Let us assume that the superconductor has infinite extension along the **y**-axis, the direction of current, and occupies the region $-w \leq x \leq w$. In the **z**-direction it can be either infinite (a slab), or very thin (a strip) with thickness $d \ll w$. With the magnetic field **B_a** applied along **z**, the flux and current density can in both cases be considered uniform in this direction. Making the common assumption that $B = \mu_0 H$, one has for a slab that

$$\mu_0 j = -\partial B / \partial x. \quad (5)$$

For a thin strip the Biot-Savart law yields

$$B(x) = B_a + \frac{d\mu_0}{2\pi} \int_{-w}^w \frac{j(u)}{u - x} du. \quad (6)$$

It is convenient to invert the latter equation, which gives¹¹

$$j(x) = \frac{2}{\pi d \mu_0} \int_{-w}^w \frac{B(x') - B_a}{x - x'} \sqrt{\frac{w^2 - x'^2}{w^2 - x^2}} dx' + \frac{I_T}{\pi d \sqrt{w^2 - x^2}}, \quad (7)$$

where I_T is the transport current.

In the numerical simulations we solve the set of equations (1), (3) for the flux-creep approach, and (1), (4) for the $E - j$ approach, respectively. The relation between B and j is taken from Eq. (5) for the case of a slab, and from Eq. (7) in the thin strip geometry. The critical current densities, j_{cU} and j_{cE} , are assumed to be B -independent.

III. NUMERICAL RESULTS

A. Comparison with exact solution

As a check of the quality of our numerical simulation scheme we compared numerical results for the $E - j$ approach with an exact analytical solution, which can be obtained in the slab case. Assume that at $t = 0$ a finite

external magnetic field is suddenly turned on. The flux density distribution can then be expressed as a function of a single scaling parameter as long as the flux fronts penetrating from opposite sides do not overlap. With $E \propto j^n$, the scaling law has the form⁹

$$B(x, t) = af(\xi), \quad \xi = (w - x)a^{-\frac{n-1}{n+1}}t^{-\frac{1}{n+1}}. \quad (8)$$

Here

$$f(\xi) = \frac{\Phi(\xi/\xi_0)}{\Phi(0)}, \quad \Phi(z) = \int_z^1 dx (1 - x^2)^{\frac{1}{n-1}}, \quad (9)$$

where ξ_0 is given by the equation

$$\xi_0^{n+1} [\Phi(0)]^{n-1} = 2n(n+1)/(n-1)$$

Note that $f(\xi_0) = 0$, and hence $\xi = \xi_0(n)$ describes the advance of the flux front.

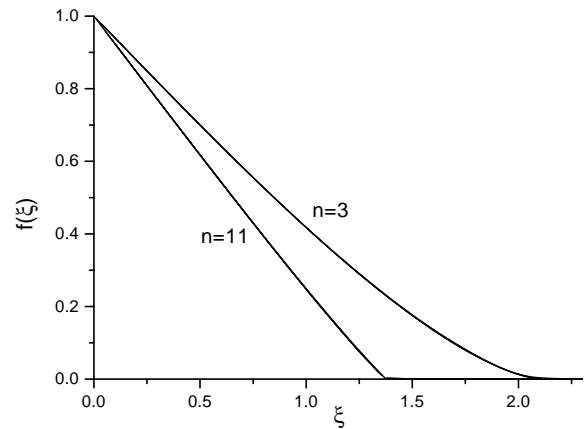


FIG. 1. Normalized B -profiles obtained by numerical simulations for a slab described by Eq. (4) with $n = 3$ and $n = 11$. The profiles, which are plotted in the scaling variable ξ defined in Eq. (8), correspond to five different times after a step has occurred in B_a . The collapse among the curves agrees fully with our analytical solution.

Shown in Fig. 1 are simulated profiles of the flux density $B(\xi)$ in a slab using $n = 3$ and $n = 11$. Both graphs contain five curves corresponding to different points in time t between 5τ and $10^4\tau$, where $\tau = B_a^2/(\mu_0 j_{cE} E_c)$. Notice the Bean model like linearity in the profiles for $n = 11$, and the clear non-linearity for $n = 3$. Shown together with these curves is also the analytic solution $f(\xi)$, given by Eq. (9). The collapse within each family of curves demonstrates an excellent agreement, and gives confidence in the numerical procedures.

B. Slab with a transport current

In the following we present simulation results assuming that a transport current, linearly increasing in time,

is passed through an initially zero-field-cooled superconductor. The choice of parameters is $dJ_T/dt = 10^{-3}j_c v_c$ where $J_T(t) = \int_{-w}^w j(x, t) dx$ is the transport current per unit height, $j_c \equiv j_{cU} = j_{cE}$, and $U_c/kT = n = 5$. Moreover, we let $E_c = 0.2v_c\mu_0j_cw$, which gives approximately the same average electric field in the superconductor for both the flux creep and $E - j$ approach.

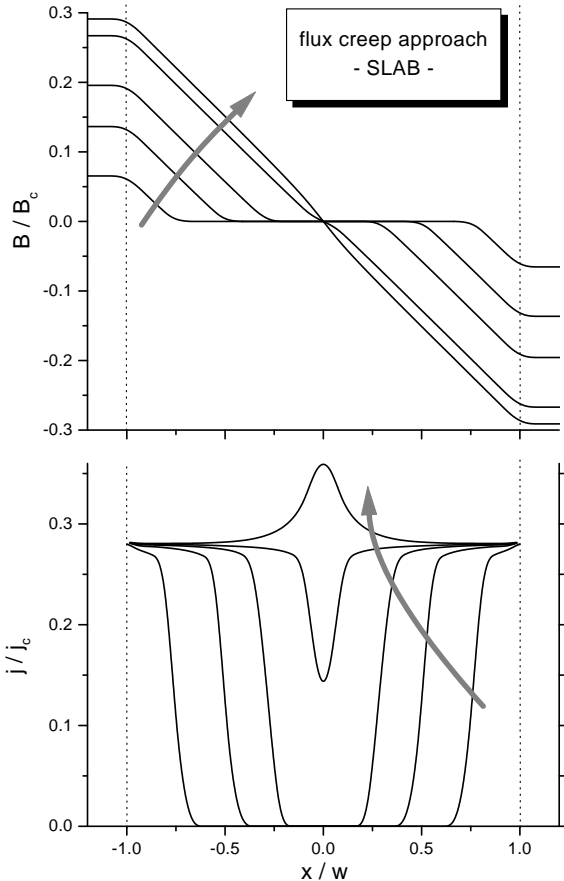


FIG. 2. Temporal evolution of current and flux density distribution in a slab with an increasing transport current. The graphs are obtained using the flux creep approach. The profiles correspond to currents $J_T/J_c = 0.07, 0.14, 0.20, 0.27, 0.29$, where $J_c = 2wj_c$. The dotted line marks the edge of the superconductor. Arrows indicate the direction of time.

Figures 2 and 3 present the time development of the current and flux density distributions in the case of a slab.¹⁰ In the flux penetrated region, which gradually expands from the edges, both approaches lead to B -profiles that are essentially linear, and a fairly constant current density. The slab has a central region where both B and j vanish. As $J_T(t)$ increases, the flux penetrates deeper, and the current becomes distributed more uniformly. Although the overall behavior resembles that of the Bean model, one can also see clear deviations, in particular in the current distributions.

The results also reveal distinct differences between the two approaches. The most prominent one is seen in the

j -distribution, where in the flux creep approach a peak develops in the center as the slab becomes fully penetrated. Another difference is visible near the edges, where the slopes in $j(x)$ are significantly larger in the $E - j$ model. Both of these features are also reflected in the B -distributions, although there only as different curvatures of the profiles.

Subsequent increase in the transport current (not shown in figures) does not change significantly the shape of distributions. In the $E - j$ approach, the current density tends to become completely uniform. In the flux creep approach, the peak in the center retains, and both $j(x)$ and $B(x)$ increase monotonously as grows the transport current, J_T .

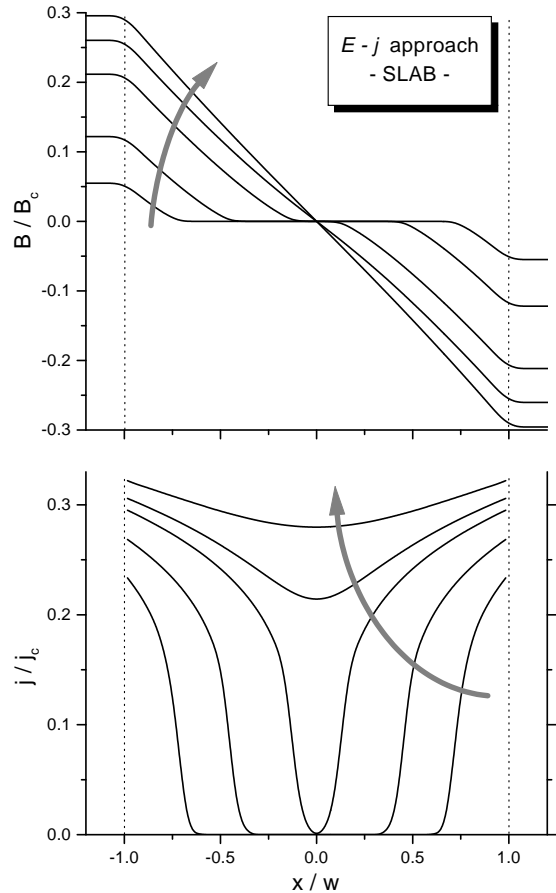


FIG. 3. Same quantities as shown in Fig. 2 only here calculated using the $E - j$ approach, and evaluated for $J_T/J_c = 0.06, 0.13, 0.21, 0.26, 0.30$.

C. Strip with a transport current

The simulated behavior of a thin strip experiencing a linearly increasing transport current I_T , is shown in Figures 4 and 5. The choice of parameters is the same as for the slab, with $dI_T/dt = 10^{-3}j_c v_c d$ except now it requires that $E_c = 0.2v_c\mu_0j_c d/\pi$, in order to give approximately the same average electric field for both the flux creep and

the $E - j$ approach. Comparing the results with the previous slab case, one immediately sees differences in the shape of the profiles. The $j(x)$ in a strip is always finite everywhere even at small currents, where the flux penetration is only partial. Furthermore, $B(x)$ is strongly nonlinear and has peaks at the edges. Both these features are well known also in the Bean model behavior for a thin strip.^{11,12}

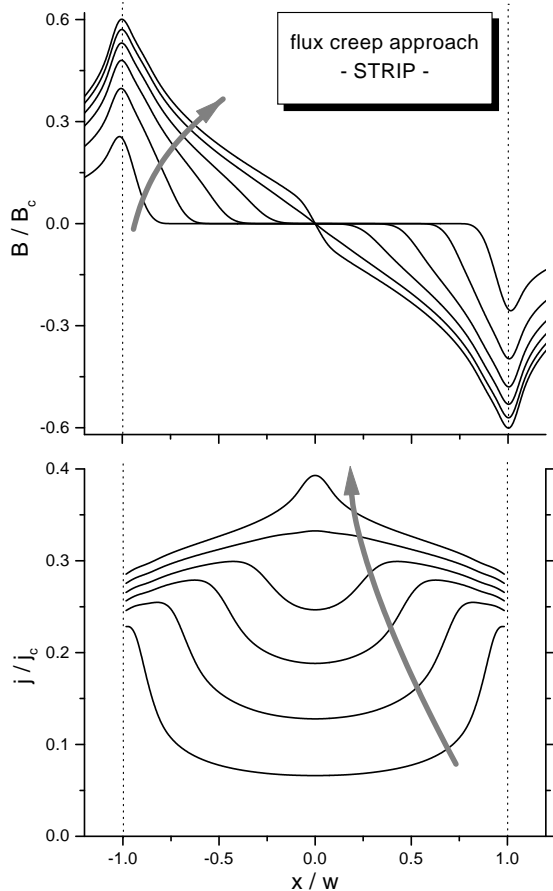


FIG. 4. Temporal evolution of flux and current density distribution in a thin strip with an increasing transport current. The flux creep approach is used to calculate the graphs. The profiles correspond to the current values $I_T/I_c = 0.10, 0.18, 0.24, 0.28, 0.31, 0.33$, where $I_c = 2wd j_c$. The dotted line marks the edge of the superconductor. Arrows indicate the direction of time.

As in the slab case, we observe also here a significant difference between the distributions obtained from the flux creep and the $E - j$ approach. Firstly, the two approaches give opposite sign for the slope of $j(x)$ in the penetrated regions near the edges. Secondly, only the creep approach leads to a central peak in $j(x)$ at large currents. Hence, while in the $E - j$ approach the $j(x)$ remains concave throughout, the creep approach predicts a gradual change from a concave to a convex profile. Contrary to the case of a slab, differences are also clearly seen in the flux distributions. In particular, the creep ap-

proach predicts a much steeper slope near the flux front.

Interestingly, we found that although the two approaches lead to quite different spatial distributions, the integral characteristics of the strip, such as current-voltage curves, are only weakly sensitive to the differences. This is demonstrated in Fig. 6, which shows the integral current-voltage curves obtained using both approaches. The curves for $n = 5$ correspond to the j -distributions shown in the previous figures. The electric field was determined as P/I_T , where the dissipated power P per unit length of the strip was calculated by integrating the product $j(x)E(x)$ over the strip cross-section.¹¹

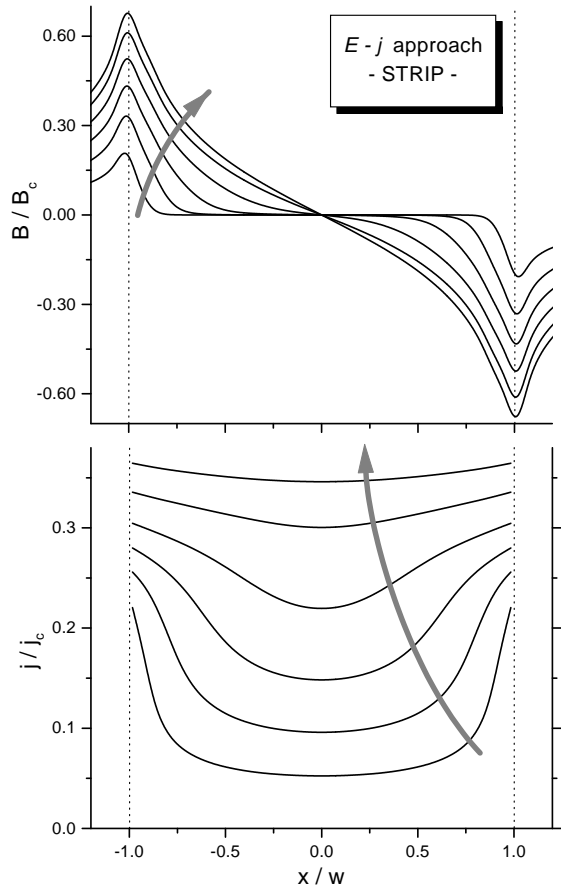


FIG. 5. Same quantities as shown in Fig. 4 only here calculated using the $E - j$ approach, and evaluated for $I_T/I_c = 0.08, 0.14, 0.20, 0.26, 0.32, 0.35$.

In the log-log plot the current-voltage curves display a clear crossover at $E \approx 0.002E_c$. At large currents the integral $E(j)$ curve shows a power law behavior $E \propto j^{n'}$, where n' is an “integral” exponent. We find that n' slightly exceeds U_c/kT in the flux creep approach. In the $E - j$ approach n' is equal to the “local” exponent n and the integral $E(j)$ curves merge the local $E(j)$ ’s shown by straight lines. At small currents the integral $E(j)$ curve also shows a power law behavior, although with a much smaller n' which seemingly does not depend on n or U_c/kT .

D. Discussion

Both approaches describe the same physical situation: in response to the transport current the flux lines enter the sample from the edge and then move some distance before getting pinned or annihilated in the sample's center. Thus, near the edges the flux motion is always more pronounced. Consequently, E has a maximum there. In the $E - j$ approach, the local current density is an explicit function of the local electric field. Therefore, $j(x)$ follows $E(x)$ and monotonously decreases from the edges towards the center. On the other hand, in the flux creep approach, $j(x)$ is related to $v(x) = E(x)/B(x)$ by Eq. (2), and, hence depends also on the flux distribution. In particular, $j(x)$ is relatively small at the strip edges where $|B|$ is maximal, see Fig. 4(a).

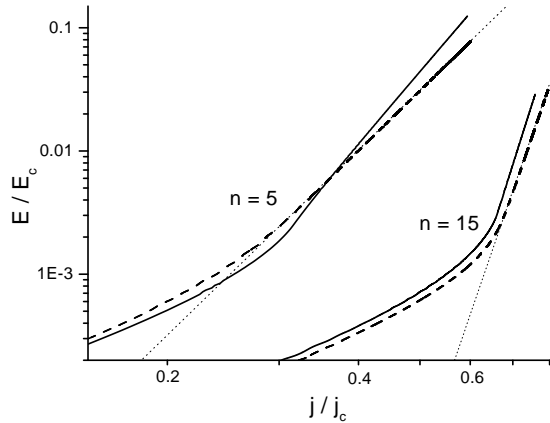


FIG. 6. Current-voltage curves for a strip obtained by numerical simulations in the flux creep approach (solid line) and in the $E - j$ approach (dashed line). Results for two different $n = U_c/kT$ are shown. Straight lines show the local $E(j)$ curve for the $E - j$ approach, Eq. (4).

IV. EXPERIMENTAL RESULTS AND DISCUSSION

A $\text{YBa}_2\text{Cu}_3\text{O}_{7-\delta}$ (YBCO) film of 200 nm thickness was prepared by dc magnetron sputtering on LaAlO_3 substrate.¹³ Using photo-lithography a strip of dimensions $500 \times 100 \mu\text{m}^2$ was formed and equipped with Ag contact pads for injection of a transport current. The current was applied in pulses of 40 ms duration while the temperature was kept at 20 K in an optical cryostat. Magneto-optical images were recorded with 33 ms exposure time during the current pulse. From the images we determine the z -component of \mathbf{B} in the plane of the ferrite garnet magneto-optical indicator, which we estimate to be located 10 μm above the YBCO film.

Shown in Fig. 7(a) are the measured B -distributions. Because of the finite distance between the indicator and the superconductor, these profiles are not easily compared to the results of the simulations. However, since

the j -profiles showed more distinct differences between the creep and $E - j$ approach, the measured B -profiles were converted to sheet current distributions, $J(x) = dj(x)$, in the strip. An inversion scheme described in Ref. 14 and further developed elsewhere¹⁵ was employed.

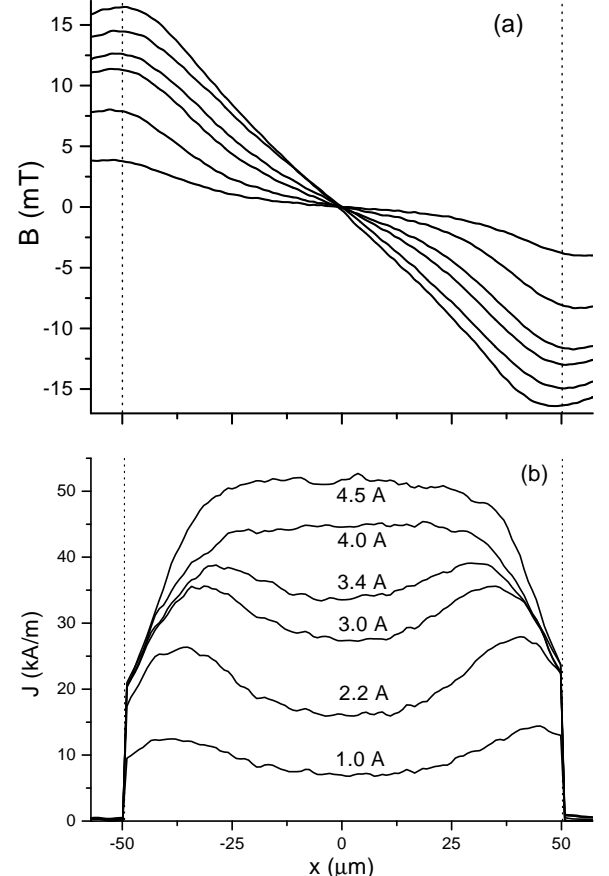


FIG. 7. (a) Flux density distributions in a thin YBCO strip carrying transport currents up to 4.5 A. The measurements were obtained using magneto-optical imaging. (b) Sheet current distributions inferred by inversion of the $B(x)$ profiles.

Profiles of the sheet current are shown in Fig. 7(b) for a range of transport currents up to 4.5 A. Evidently, they fit quite well to the simulated results of the creep approach shown in Fig. 4. In particular, one easily recognizes the characteristic change from a concave to a convex current distribution as I_T increases. The $E - j$ approach, on the other hand, appears not to be able to give an adequate description of the flux dynamics in the present experiment.

Although being the better model, one can still see considerable discrepancies between the experimental curves and the flux-creep approach simulations. One example is the peak of $j(x)$ in the strip center at large currents, a feature the experiments could not reproduce. Unfortunately, a current of 4.8 A caused fatal damage to the sample, and we were not able to measure distributions

under the conditions where a central peak might become apparent.

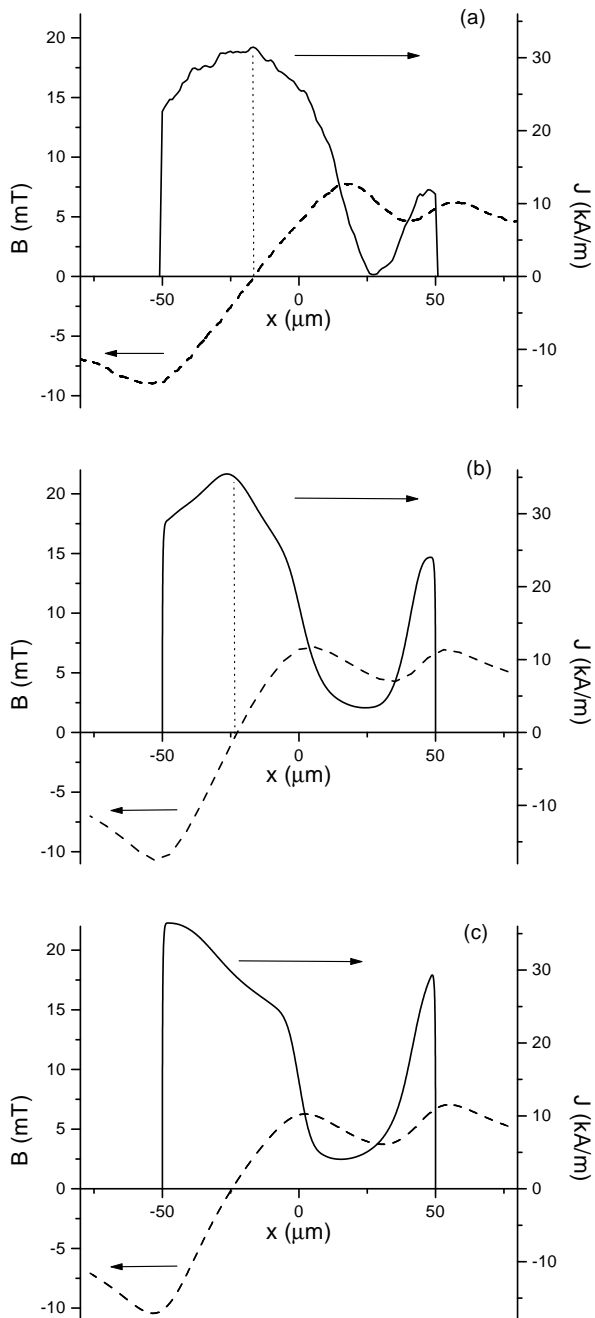


FIG. 8. Sheet current (solid lines) and the flux density (dashed lines) distributions in a thin strip: experiment (a) and simulations in the flux creep approach (b) and simulations in the $E - j$ approach (c). The strip was first exposed to a very high magnetic field which subsequently was reduced to zero. After that a transport current of 2 A was applied. The experimental data were obtained from magneto-optical images of a YBCO strip.

As an alternative way to create a peak in J where B

changes sign, we carried out a different experiment. Here the strip (a new YBCO sample prepared by the same method) was initially in the remanent state after first being exposed to a very high magnetic field. After that the strip was subjected to a transport current of 2 A. The resulting flux and current distributions are shown in Fig. 8(a). One sees that in the left half of the strip there is a wide region with a large and nearly constant current density. Within this region one finds that $J(x)$ indeed has a peak located close to the point where $B = 0$.

A new set of simulations was made for this special state with combined magnetization currents and I_T . The simulations aimed to reproduce the exact experimental steps: First, the strip was exposed to a perpendicular magnetic field applied as a pulse of 70 mT amplitude with 1 s of linear increase and 1 s of linear decay. Then, after one more second, the strip was subjected to a transport current pulse with 1 ms rise time. During the current pulse, 20 ms after turn-on, the magneto-optical image was taken. For this particular time, Figs. 8(b) and (c) present the numerically obtained distributions for the flux creep approach and $E - j$ approach, respectively. The following model parameters were used: $n = U_c/kT = 5$, $I_c = 25$ A, and $v_c = 10$ m/s. Again, only the flux creep approach gives a peak in the current profile, and now we find an excellent agreement with the experimental results.

A remaining discrepancy between the flux-creep approach simulations and the experimental curves is that the gradient of $J(x)$ near the strip edge is larger in the experiments. This holds true also for simulations made with other values of the power U_c/kT . We believe that our photo-lithographic technology does not reduce the film quality much more than up to a distance 1-2 μ m from the edge. This is also consistent with the magneto-optical images, which show that the current flow along the strip is highly uniform on scales larger than 5 μ m. Therefore, the discrepancy between experiment and simulations indicates that the vortex behavior is more complicated than assumed in the present flux creep model. The experimentally observed suppression of J near the edge where $|B|$ is maximal, can be interpreted as a $|B|$ -induced reduction of the critical current density j_{cU} , or the pinning energy U_c . This interpretation, however, fails to account for a similar suppression of J observed previously in the remanent state after current pulse.¹⁶ An alternative explanation able to cope with both observations is a heat dissipation due to vortex motion which is always most intensive near the strip edges.

V. CONCLUSIONS

Numerical simulations have been carried out in order to compare two commonly accepted approaches for analysis of flux motion in superconductors; (i) the flux creep approach, and (ii) the approach based on a non-linear $E(j)$ curve. We have shown that if the critical cur-

rent density is field-independent, these approaches predict similar but also distinctly different current and flux distributions. The difference is most pronounced in the regions where the local flux density B is small. The simulation results were compared with the real current distributions in a YBCO strip carrying a transport current. The experimental data were obtained by using magneto-optical imaging. The comparison shows clearly that the flux creep approach provides the better description of the flux motion in the strip.

ACKNOWLEDGMENTS

The financial support from the Research Council of Norway (NFR), and from NATO via NFR is gratefully acknowledged. We are grateful to Bjørn Berling for a many-sided help and to E. H. Brandt for a discussion.

* Email: t.h.johansen@fys.uio.no

¹ Y. Yeshurun and A. P. Malozemoff, Phys. Rev. Lett. **60**, 2202 (1988).

² Y. Yeshurun, A. P. Malozemoff, and A. Shaulov, Rev. Mod. Phys. **68**, 911 (1996).

³ H. G. Schnack, R. Griessen, J. G. Lensink, C. J. van der Beek, and P. H. Kes, Physica C **197**, 337 (1992).

⁴ L. Burlachkov, D. Giller, and R. Prozorov, Phys. Rev. B **58**, 15067 (1998).

⁵ A. Gurevich and E. H. Brandt, Phys. Rev. Lett. **73**, 178 (1994).

⁶ E. H. Brandt, Phys. Rev. B **49**, 9024 (1994).

⁷ E. H. Brandt, Phys. Rev. B **58**, 6506 (1998).

⁸ The approaches would become equivalent for a special choice of the parameters involved. In particular, if E_c is proportional to B , or if the critical current densities are related to each other as $j_{cE}(B) = j_{cU}(B)B^{-1/n}$ with $n = U_c/kT$.

⁹ Y. M. Galperin and T. H. Johansen, unpublished.

¹⁰ Movies of time development of $B(x)$, $j(x)$, and $E(x)$ distributions are presented at <http://www.fys.uio.no/faststoff/ltl/results/creep>

¹¹ E. H. Brandt, and M. Indenbom, Phys. Rev. B **48**, 12893 (1993).

¹² E. Zeldov, J. R. Clem, M. McElfresh, and M. Darwin, Phys. Rev. B **49**, 9802 (1994).

¹³ S. F. Karmanenko, V. Y. Davydov, M. V. Belousov, R. A. Chakalov, G. O. Dzjuba, R. N. Il'in, A. B. Kozyrev, Y. V. Likholetov, K. F. Njakshev, I. T. Serenkov, O. G. Vendic, Supercond. Sci. Technol. **6**, 23 (1993).

¹⁴ T. H. Johansen, M. Baziljevich, H. Bratsberg, Y. Galperin, P. E. Lindelof, Y. Shen, and P. Vase, Phys. Rev. B **54**, 16 264 (1996).

¹⁵ A. V. Bobyl et al., unpublished.

¹⁶ M. E. Gaevski, A. V. Bobyl, D. V. Shantsev, S. F. Karmanenko, Y. M. Galperin, T. H. Johansen, M. Baziljevich, H. Bratsberg, Phys. Rev. B **59**, 9655 (1999)